Colloids and Surfaces B: Biointerfaces 234 (2024) 113730

Contents lists available at ScienceDirect

Colloids and Surfaces B: Biointerfaces

journal homepage: www.elsevier.com/locate/colsurfb

Design of fluorinated stealth poly(ε-caprolactone) nanocarriers

Beatrice Lucia Bona [a], Prescillia Lagarrigue [a,b,1], Cristina Chirizzi [a,2], Maria Isabel Martinez Espinoza [a], Christian Pipino [a], Pierangelo Metrangolo [a], Francesco Cellesi [a,b], Francesca Baldelli Bombelli [a,*]

[a] SupraBioNanoLab, Department of Chemistry, Materials, and Chemical Engineering "Giulio Natta", Politecnico di Milano, Milano 20131, Italy
[b] Department of Chemistry, Materials, and Chemical Engineering "Giulio Natta", Politecnico di Milano, Milano 20131, Italy

ARTICLE INFO

Keywords:
Fluorine
^{19}F NMR
Polymer
Nanoparticles
Protein corona
Drug delivery

ABSTRACT

The covalent functionalization of polymers with fluorinated moieties represents a promising strategy for the development of multimodal systems. Moreover, polymer fluorination often endows the resulting nanocarriers with improved colloidal stability in the biological environment. In this work, we developed fluorinated pegylated (PEG) biodegradable poly(ε-caprolactone) (PCL) drug nanocarriers showing both high colloidal stability and stealth properties, as well as being (^{19}F)-Nuclear Magnetic Resonance (NMR) detectable. The optimized nanocarriers were obtained mixing a PEG-PCL block copolymer with a nonafluoro-functionalized PCL polymer. The role of PEGylation and fluorination on self-assembly and colloidal behavior of the obtained nanoparticles (NPs) was investigated, as well as their respective role on stealth properties and colloidal stability. To prove the feasibility of the developed NPs as potential ^{19}F NMR detectable drug delivery systems, a hydrophobic drug was successfully encapsulated, and the maintenance of the relevant ^{19}F NMR properties evaluated. Drug-loaded fluorinated NPs still retained a sharp and intense ^{19}F NMR signal and good relaxivity parameters (i.e., T_1 and T_2 relaxation times) in water, which were not impaired by drug encapsulation.

1. Introduction

In the last decades, the application of nanotechnology into medicine emerged as a promising approach for the development of innovative nanoparticle (NP)-based therapeutics [1]. However, due to the lack of a full understanding on how NPs behave inside the human body, only few of these therapeutics have reached clinical applications [2]. Consequently, development of multifunctional NPs combining the therapeutic action with the possibility of tracking them in-vivo with different imaging methods has been extensively investigated [3–5]. Among non-invasive imaging techniques, Fluorine-19 (^{19}F)-Magnetic Resonance Imaging (MRI) has emerged as a powerful quantitative detection modality [6–11]. Thanks to the lack of detectable endogenous organic fluorine in tissues, ^{19}F-MRI does not suffer any background signal [8,12]. This allows to obtain high resolution hot-spot images that add a second independent information (e.g., biodistribution) to the anatomical one provided by ^{1}H-MRI [6,8].

The covalent functionalization of biocompatible polymers with fluorinated ligands is considered a promising strategy for the development of ^{19}F-MRI active nanocarriers with unique physicochemical properties [7,9,13–15]. By playing on different types of fluorinated tags and polymeric scaffolds, it is possible to combine a degree of fluorination suitable for imaging applications with the possibility to finely tune the system biodegradability, biocompatibility, and hydrophilicity [9,14,16].

Moreover, thanks to their intrinsic amphiphilic nature, most fluoropolymers spontaneously self-assemble in aqueous solutions, with the possibility to encapsulate drugs of hydrophobic nature [13,17,18]. Fluorination is also reported to enhance NP stability both in water and phospholipid phase [17], while improving intracellular delivery and endosomal escape [19–21].

In fluorine chemistry, the use of short and branched rather than linear fluorinated ligands has been reported to be advantageous in terms of easy of functionalization, biodistribution and bioaccumulation [9]. Additionally, fluorination is highly exploited for detecting and quantifying nanomedicines and pharmaceuticals through (^{19}F)-Nuclear

* Corresponding author.
E-mail address: francesca.baldelli@polimi.it (F. Baldelli Bombelli).
[1] CIRIMAT, Université Toulouse 3 Paul Sabatier, Toulouse INP, CNRS, Université de Toulouse, 118 Route de Narbonne, 31062 Toulouse cedex 9, France.
[2] Neuroradiology Unit, Fondazione IRCCS Neurologico Carlo Besta, Milano 20100, Italy.

https://doi.org/10.1016/j.colsurfb.2023.113730
Received 28 September 2023; Received in revised form 21 December 2023; Accepted 24 December 2023
Available online 26 December 2023

Magnetic Resonance (NMR) spectroscopy, as well as improving the encapsulation efficacy of fluorinated drugs, as we have recently demonstrated [13]. For these reasons, covalent functionalization of polymers with branched fluorinated ligands can be considered as an interesting strategy for the development of drug nanocarriers potentially detectable by ^{19}F NMR [13].

When dealing with the development of ^{19}F NMR probes, it is crucial to ensure the mobility of the fluorinated chains in order to achieve a suitable transverse relaxation time (T_2), which is essential for a good signal. In this sense, polymer functionalization with fluorinated ligands bearing a reduced number of fluorinated branches is reported to maintain fluorine mobility after self-assembly, thus avoiding quenching of the NMR signal and still guaranteeing a suitable amount of fluorine atoms for the ^{19}F NMR analytical needs [13,16]. In this work, we developed pegylated biodegradable poly ε-caprolactone (PCL) nanoparticles (NPs) functionalized with a branched nonafluoro moiety as ^{19}F NMR detectable drug delivery vehicles, which showed high colloidal stability. The Food and Drug Administration-approved PCL and polyethylene glycol (PEG), and their amphiphilic block-copolymers are among the most attractive materials for biomedical applications [22]. This is due to their good biocompatibility, (partial) biodegradability, ease of functionalization, and the possibility to finely tune their molecular architectures affecting the resulting self-assembly and physicochemical properties [23,24].

To design detectable NPs with improved colloidal stability and stealth properties, we primarily studied the role of fluorination and pegylation on self-assembly and colloidal behavior of PCL-based NPs in physiological conditions and in the presence of proteins. NPs were formulated from mixtures in different ratios of a PEG-PCL copolymer with PCL polymers terminating either with a nonafluoro (FPCL) or with a trimethylated moiety (HPCL), as non-fluorinated control. HPCL and FPCL-NPs prepared at different PEG surface density were studied by dynamic light scattering (DLS) for determining their colloidal stability. NP attitude to form a protein corona (PC), i.e., the layer of proteins interacting with the NP surface and strongly affecting the fate of NP in-vivo [25–27], was also investigated in the biological environment. This characterization defined the best polymer composition for obtaining highly stable and stealth NPs. The biocompatibility of the selected NPs was also evaluated. Subsequently, to validate the feasibility of selected NPs as drug delivery systems, dexamethasone, as an example of hydrophobic drug, was encapsulated in the obtained NPs, which retained colloidal stability and showed effective encapsulation efficiency. Moreover, the developed fluorinated NPs, studied by ^{19}F NMR, exhibited promising detectability and imaging properties in terms of intensity of the peak and relaxation times.

2. Materials and methods

2.1. Materials

ε-Caprolactone (ε-CL) was distilled before use. 3-(Nonafluoro-*tert*-butyl)propan-1-ol ($(CF_3)_3C$-$(CH_2)_2$-OH), stannous 2-ethyl hexanoate (Sn$(Oct)_2$), dichloromethane (DCM), methanol, deuterated chloroform ($CDCl_3$), propargyl alcohol, anhydrous toluene, polyethylene glycol (2000 g/mol, PEG2k), 3,3-dimethyl-1-butanol ($(CH_3)_3C$-$(CH_2)_2$-OH) were purchased from Sigma-Aldrich (Merck).

Trifluoroacetic acid (CF_3COOH), phosphate buffered saline (PBS), Fetal Bovine Serum (FBS) (TMS-013), sucrose, β-mercaptoethanol, sodium dodecyl sulphate (SDS), Trizma Base (Tris), dexamethasone ($C_{22}H_{29}FO_5$), and sucrose were purchased from Merck. Dulbecco's modified eagle medium (DMEM) was purchased from Gibco BRL Life Technologies. 2x Laemmli Sample Buffer, 40 % acrylamide/bis-acrylamide (37.5:1) solution, *N,N,N′,N′*-tetramethylenediamine (TEMED), Colloidal Coomassie Blue, Precision Plus Protein TM Standards Unstained and Dual Colors were purchased from Bio- Rad® Laboratories. Ultrapure type-I Milli-Q water (MilliQ water) (18.2 mΩ/cm) was obtained by a Simplicity® water purification system (Merk, Germany).

Human mesenchymal stem cells (MSCs) for cellular study were generously provided by Dr. Daniela Lisini from the Cell Therapy Production Unit-UPTC and Cerebrovascular Diseases Unit, Fondazione IRCCS Istituto Neurologico Carlo Besta, Milan, Italy.

2.2. Polymer synthesis

2.2.1. Polymer characterisation

^{1}H-NMR spectra were recorded on a Bruker AVANCE 400 MHz instrument at 298 K. Chemical shifts (δ) are reported in ppm downfield from the deuterated solvent as internal standard, coupling constants (J) are in Hz. The number-average molecular weight ($Mn_{,SEC}$) and dispersity (Đ =Mw/Mn) values of the polymers were evaluated by Size Exclusion Chromatography (SEC), which was carried out with JASCO® instrument equipped with a refractive index detector (RI-2031 Plus, Jasco) using 3 Agilent PL gel columns, 5 μM particle size, 300 × 7.5 mm (MW range: 5×10^2 to 17×10^5 g/mol). THF was chosen as eluent at a flow rate of 1 mL/min at 35 °C. The SEC samples were dissolved in THF at a concentration of 4 mg mL^{-1}, filtered through 0.22 μm PTFE syringe filters and injected using a Jasco AS-2055 Plus autosampler. The instrument was calibrated using polystyrene standards (by RESTECK and Sigma-Fluka).

2.2.2. Synthesis of polyethylene glycol-polycaprolactone (PEG-PCL)

PEG-PCL was synthesized by ring-opening polymerization of distilled ε-caprolactone (ε-CL) under nitrogen atmosphere in a round bottom flask using polyethylene glycol (2000 g/mol, PEG2k) as initiator and stannous 2-ethyl hexanoate ($Sn(Oct)_2$) as catalyst. 2 g of ε-CL (17.52 mmol) were placed in a dried round bottom flask and degassed by three nitrogen/vacuum cycles. PEG2k (700.8 mg, 0.35 mmol) and $Sn(Oct)_2$ (9.92 mg, 0.025 mmol) were then added to the monomer under nitrogen flux and stirring. The reaction was then performed at 115 °C for 1 day under nitrogen atmosphere. At the end of the reaction, the crude mixture was dissolved with CH_2Cl_2 and dropped in cold methanol (methanol/CH_2Cl_2: 50/1 v/v). The mixture was kept overnight in the freezer at –20 °C before recovering the polymer by filtration and washing. Finally, the polymer was dried under reduced pressure. Conversion: 88 %, Yield > 90 %.

^{1}H NMR (400 MHz, $CDCl_3$) δ (ppm): 4.08–4.04 (t, 2 H (n-1), -C*H*$_2$-OC(O)-), 3.64 (t, 2 H, C*H*$_2$-OH), 3.37 (s, 3 H, *H*$_3$C-O), 2.37–2.29 (m, 2 H n, -OC(O)-C*H*$_2$-), 1.70–1.55 (m, 4 H n, OC(O)-CH$_2$-C*H*$_2$), 1.45–1.24 (m, 2 H n, -CH$_2$-C*H*$_2$-CH$_2$), where n is the PCL degree of polymerization. $M_{n,(PCL)\,NMR}$ = 5900 g/mol, $M_{n,NMR}$ = 7900 g/mol $M_{n,SEC}$ = 10,400 g/mol, Đ = 1.1.

2.2.3. Synthesis of fluorinated polycaprolactone (FPCL)

FPCL was synthesized by ring-opening polymerization of distilled ε-caprolactone (ε-CL) under nitrogen atmosphere in a round bottom flask using 3(nonafluoro-*tert*-butyl)propan-1-ol ($(CF_3)_3C$-$(CH_2)_2$-OH) as initiator and stannous 2-ethyl hexanoate ($Sn(Oct)_2$) as catalyst. 2 g of ε-CL (17.52 mmol) and 67.7 mg of $(CF_3)_3C$-$(CH_2)_2$-OH (0.25 mmol) were placed in a dried round bottom flask and degassed by three nitrogen/vacuum cycles. Then, the catalyst $Sn(Oct)_2$ (7.09 mg, 0.0175 mmol) was added to the reaction mixture. The reaction was performed at 130 °C for 66 h under nitrogen atmosphere. The crude was dissolved with CH_2Cl_2 and purified by precipitation, by dropping it in cold methanol (methanol/CH_2Cl_2: 50/1 v/v). The precipitated polymer was recovered by filtration and washed with cold methanol, and dried under reduced pressure. Conversion: 83 %, Yield >90 %.

^{1}H NMR (400 MHz, $CDCl_3$) δ (ppm): 4.08–4.04 (t, 2 H (n-1), -CH$_2$-OC(O)-), 3.64 (t, 2 H, CH$_2$-OH), 1.70–1.55 (m, 4 H n, OC(O)-CH$_2$-CH$_2$), 1.45–1.24 (m, 2 H n, -CH$_2$-CH$_2$-CH$_2$), where n is the PCL degree of polymerization. ^{19}F NMR ($CDCl_3$) δ (ppm): 66.8 (s, 9 F, $(CF_3)_3$). $M_{n,NMR}$ = 4300 g/mol, $M_{n,SEC}$ = 6000 g/mol, Đ = 1.46.

2.2.4. Synthesis of trimethylated polycaprolactone (HPCL)

PCL with a terminal 3,3-dimethyl-1-butanol ($(CH_3)_3C$-$(CH_2)_2$-OH) was synthesized by ring-opening polymerization of distilled ε-caprolactone (ε-CL) under nitrogen atmosphere in a round bottom flask using 3,3-dimethyl-1-butanol as initiator, stannous 2-ethyl hexanoate (Sn $(Oct)_2$) as catalyst, and anhydrous toluene as solvent. 5 g of ε-CL (43.8 mmol) and 10 mL of anhydrous toluene were placed in a dried round bottom flask and degassed by three nitrogen/vacuum cycles. Then, 64 mg of $(CH_3)_3C$-$(CH_2)_2$-OH (0.63 mmol) the initiator and the catalyst Sn $(Oct)_2$ (18 mg, 0.044 mmol) were added to the reaction mixture. The reaction was performed at 110 °C for 48 h under nitrogen atmosphere and reflux. The crude was purified by precipitation, dropping the solution in cold methanol (methanol/toluene: 50/1 v/v). The precipitated polymer was recovered by filtration and washed with cold methanol, and dried under reduced pressure. Conversion: 72 %, Yield > 90 %.

^{1}H NMR (400 MHz, $CDCl_3$) δ (ppm): 4.08–4.04 (t, 2 H (n-1), -C*H*$_2$-OC(O)-), 3.64 (t, 2 H, C*H*$_2$-OH), 1.70–1.55 (m, 4 H n, OC(O)-CH_2-CH_2), 1.45–1.24 (m, 2 H n, -CH_2-CH_2-CH_2), 0.94 (s, 9 H, $(CH_3)_3$-CH_2), where n is the PCL degree of polymerization. $M_{n,NMR}$ = 4800 g/mol, $M_{n,SEC}$ = 8000 g/mol, Đ = 1.42.

2.3. NP preparation and characterization

Three different classes of mixed-polymers NPs were prepared; NPs based on a mixture of HPCL and FPCL in different weight ratios (1:0, 1:1, 3:7, 1:4, 0:1), NPs based on a mixture of PEG-PCL and HPCL in different weight ratios (1:4, 3:7, 1:1, 4:1), NPs based on a mixture of PEG-PCL and FPCL in different weight ratios (1:4, 3:7, 1:1, 4:1), and NPs made with 100 % PEG-PCL. A summary of prepared NPs is reported in Table 1.

NPs were formulated by a nanoprecipitation method in surfactant-free conditions using 1:1 acetone/water volume ratio, adapting a previously reported procedure [23]. Briefly, the procedure consisted of the drop-wise addition of 1 mL of the desired polymer blend solution in acetone (total polymer concentration: 10 mg mL^{-1}) to 1 mL of MilliQ water (filtered with a 0,2 μm filter). The obtained emulsion was left stirring for 5 min at controlled room temperature (*r.t.*) (25 °C), and then the organic solvent was fully removed under reduced pressure (35 °C). NPs were characterized by dynamic light scattering (DLS), and Zeta Potential (ZP) analysis. DLS measurements were performed on an ALV apparatus equipped with ALV-5000/EPP Correlator, special optical fiber detector and ALV/CGS-3 Compact goniometer (ALV-GmbH, Langen/-Germany). The light source is He–Ne laser (l = 633 nm), 22 mW output power. Measurements were performed at 25 °C. Approximately 1 mL of 1:10 sample solution in MilliQ water or in DMEM + 10 % FBS was transferred into the cylindrical Hellma scattering cell.

Data analysis was performed according to standard procedures and auto-correlation functions - measured at 90° scattering angle (θ) - were analyzed through a constrained regularization method, CONTIN, for obtaining NPs intensity weighted hydrodynamic radius (R_H) distribution. Polydispersity indexes (PDI) were obtained by cumulant fitting.

ZP analyses were performed on a Zetasizer Nano ZS apparatus (Malvern Instruments, Malvern, Worcestershire, UK), equipped with a 633 nm laser at 25 °C on approximately 1 mL of 1:10 sample solution in MilliQ water.

For DLS an ZP analyses, each measurement was repeated three times, and for each sample three batches were independently measured. Standard deviations were calculated accordingly.

^{19}F NMR properties of NPs based on 50 % PEG-PCL/FPCL were evaluated using a Bruker AV400 spectrometer. Analyses were performed at *r.t.* and chemical shifts are reported in part per million (ppm). Trifluoroacetic acid (TFA) was added as external standard, with chemical shift set at –75.48 ppm. ^{19}F longitudinal (T_1) and transverse (T_2) relaxation times measurements were recorded at 305 K on a Bruker AV400 spectrometer operating at 400 MHz for the ^{1}H nucleus. The inversion recovery and the CPMG pulse sequences were used for the measurements of T_1 and T_2, respectively.

Table 1
Summary of the prepared NPs.

Type of NPs	HPCL % w/w	FPCL % w/w	PEG-PCL % w/w
100 % HPCL	100	0	0
50 % HPCL/FPCL	50	50	0
30 % HPCL/FPCL	30	70	0
20 % HPCL/FPCL	20	80	0
100 % FPCL	0	100	0
20 % PEG-PCL/HPCL	80	0	20
30 % PEG-PCL/HPCL	70	0	30
50 % PEG-PCL/HPCL	50	0	50
80 % PEG-PCL/HPCL	20	0	80
20 % PEG-PCL/FPCL	0	80	20
30 % PEG-PCL/FPCL	0	70	30
50 % PEG-PCL/FPCL	0	50	50
80 % PEG-PCL/FPCL	0	20	80
100 % PEG-PCL	0	0	100

2.4. Protein corona studies

NPs were diluted 1:5 in DMEM + 10 % FBS and incubated for 1 h at 37 °C. NP-PC complexes were isolated using a sucrose cushion procedure with three subsequent centrifugation cycles (18,000 rpm, 4 °C, 30 min) adapting the protocol reported by D. Docter *et al.* [28] After each centrifugation cycle, the obtained pellet was resuspended in 500 μL of MilliQ water and DLS analysis was performed to confirm NP stability and the effectiveness of the purification protocol (see paragraph 2.3 for instruments details). Purified complexes were analyzed by Sodium Dodecyl Sulphate - PolyAcrylamide Gel Electrophoresis (SDS-PAGE). Upon last centrifugation cycle, each NP pellet was recovered and resuspended in 500 μL of MilliQ water and then dried under vacuum. The dried pellet was resuspended in 67 μL of Laemmli Buffer + 5 % beta-mercaptoethanol and 20 μL of this solution were loaded on a 12 % polyacrylamide gel. Coomassie blue staining overnight followed by destaining in a 7 % acetic acid solution in water was performed to visualize protein bands. DMEM + 10 % FBS without incubating NPs was used as control. Specifically, it was diluted 1:5 with MilliQ water and it was subject to the same centrifugation and SDS-PAGE protocol used for NPs. Resuspension in MilliQ water after each centrifugation cycle as well all the subsequent steps were performed pretending to have a pellet. This allowed to exclude eventual free protein contamination in NPs pellet deriving from the centrifugation procedure, and possibly resulting in unreliable data about PC formation.

2.5. Cell viability studies

MSCs were isolated from lipoaspirates of adipose tissue (AT) and cultured in DMEM low glucose (Euroclone, Milan, Italy) supplemented with 5 % adjunct protein material for ex vivo expansion, as previously described [29].

For biocompatibility experiments, MSCs were seeded at a density of 2.1×10^4 cells/cm^2 in a 6-well plate and incubated with 0.4 mM of both 20 % and 50 % PEG-PCL/FPCL NPs at 37 °C and 5 % CO_2 for 24 h. Following NPs incubation, cell viability was assessed by flow cytometry (MACSQuant® Analyzer 10, Miltenyi Biotec, Bergisch Gladbach, Germany) with 7-Aminoactinomycin D (7-AAD) staining (BioLegend, Calif). As blank control, cells were treated with an equal volume of MilliQ water or culture medium and underwent the same experimental procedures. For the experiment a single batch of NPs was used, and each measurement has been repeated three times. Standard deviations were calculated accordingly.

2.6. Drug-loaded NP preparation and characterization

Dexamethasone (DEX) was solubilized in acetone to prepare a

solution of 0.2 mg mL^{-1} concentration. Then the desired polymer mixture (respectively 50 % PEG-PCL/HPCL and 50 % PEG-PCL/FPCL) was solubilized in 1 mL of DEX solution (total polymer concentration 10 mg mL^{-1}). Then the polymer/drug mixture was added dropwise to 1 mL of filtered (0,2 μm filter) MilliQ water. The obtained emulsion was left stirring for 5 min at controlled *r.t.* (25 °C) and then the organic solvent was fully removed under reduced pressure as for drug-free NPs. To remove the eventual unloaded drug, the obtained dispersion was mildly centrifuged (17 rcf, 3 min). NPs were characterized by DLS as described in paragraph 2.3 and by Transmission Electron Microscopy (TEM). TEM bright field images were acquired using a DeLong instruments LVEM5 (Delong instruments a. s. Czech Republic), equipped with a Field Emission Gun filament operating at 5 kV. NPs diluted 1:5 in MilliQ water were placed on a 200-mesh carbon-coated cupper grid and air dried before analysis. No negative staining was used. TEM deriving size distribution elaboration was done by ImageJ. DEX content was determined by High Performance Liquid Chromatography (HPLC) analyses following a previously reported procedure [13]. Briefly, lyophilized NPs were dissolved in 1 mL of acetonitrile and then diluted 1:10 in acetonitrile. Each sample was injected (20 μL) in a C18 reversed-phase chromatography column at 25 °C with a flow rate of 1 mL/min in a solution of acetonitrile/water 1:1. The DEX peak was detected after 3 min. The detection wavelength was set at 235 nm. The calibration curve was previously obtained with different DEX concentrations (1, 0.5, 0.1, 0.01, 0.001 mg mL^{-1}). Drug loading (DL%) and encapsulation efficiency (EE%) values associated to each NP type were calculated according to the following equations: DL% = 100 x (weight of drug encapsulated)/(weight of drug encapsulated + weight of polymer NPs), where at the denominator it was considered the weight of drug loaded NPs measured after freeze drying and not the theoretical one, and EE% = 100 x (weight of drug encapsulated in polymer NPs)/(weight of drug used in encapsulation method) [13]. Each sample was measured three times and three batches of the same sample were measured. Standard deviations were calculated accordingly. Analyses were performed on a JASCO® HPLC equipped with: 2057 autosampler; RI-2031 refraction index detector; UV/Vis detector, CO-2060 plus oven column; PU-2080 pump; MD-2018 photodiode array PDA detector; C18 column (5 mm particle size) 150 mm × 4.6 mm (length x diameter). Mobile phase consisted of 1:1 (v/v) water/ acetonitrile. Evaluation of the drug concentration was done using the UV/Vis detector. ^{19}F NMR properties of 50 % PEG-PCL/FPCL drug-loaded NPs were evaluated as reported in paragraph 2.3.

3. Results and discussion

3.1. Polymer synthesis

PCL-based functional (co)polymers were synthesized through a standard ring opening polymerization of the monomer (ε-CL) with stannous 2-ethyl hexanoate ($Sn(Oct)_2$) as catalyst [23,24,30]. Targeted degrees of polymerization (DP=30–50) were selected to obtain PCL with a molecular weight distribution between 5000 and 8000 g/mol, which provide the required chain length for guaranteeing NP self-assembly, colloidal stability, and drug loading [31,32].

Depending on the different hydroxyl-bearing compounds used as initiator (PEG2k, $(CF_3)_3C$-$(CH_2)_2$-OH, $(CH_3)_3C$-$(CH_2)_2$-OH), the polymeric precursors for the preparation of the NPs were obtained (Fig. 1). PEG2K (with a number average molar mass M_n = 2000 g/mol) was chosen to produce NPs with good stealth characteristics for in vivo applications [33]. The amphiphilic PEG-PCL block copolymer was synthesized to obtain pegylated NPs or micelles, FPCL presented a terminal nonanofluoro moiety, while PCL with a terminal trimethylated moiety (HPCL) was used as the non-fluorinated counterpart.

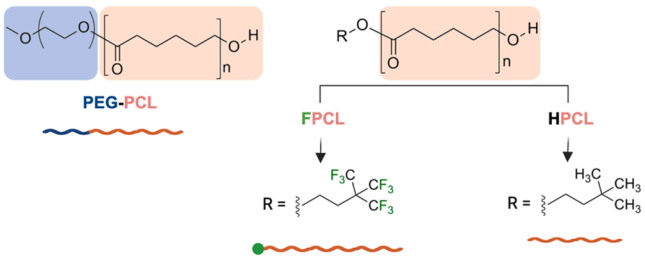

Fig. 1. Schematic representation of the synthesized polymers.

3.2. Drug-free NPs design: study of the role of fluorine and PEG on NPs colloidal behaviour

Non-pegylated NPs were formulated by mixing different percentages (w/w) of synthesized FPCL with HPCL, while pegylated NPs were prepared by mixing PEG-PCL and FPCL/HPCL polymers in different percentages (w/w). A scheme of all the different types of prepared NPs is reported in Fig. 2. Non-pegylated NPs colloidal behavior was evaluated in water by DLS and ZP. Pegylated NPs colloidal behavior was evaluated in water by DLS and ZP and in protein containing media by DLS.

The first step for the design of effective fluorinated drug delivery systems was to selectively define the role of fluorine on NPs colloidal behavior. To this aim, non-pegylated NPs prepared using a mixture of HPCL and FPCL at different percentages in weight (FPCL respectively at 0 %, 50 %, 70 %, 80 %, 100 % in the mixture) were used. Colloidally stable PCL NPs without any steric PEG stabilization were obtained thanks to the presence of few residual carboxylic groups in the PCL chains, obtained via a reduced control of the anhydrous polymerization conditions, avoiding inconvenient distillation of reagents and solvents and completely moisture-free processes. This was confirmed by ZP analysis as the NP dispersions in water showed values varying between – 40 ± 2 mV and – 30 ± 2 mV, confirming NP colloidal stability due to electrostatic repulsions.

Considering the small size of the fluorinated moiety with respect to the PCL block, fluorine should not consistently affect the overall properties of the polymer. Therefore, regardless of the ratio between HPCL and FPCL in the formulation, NPs should self-assemble with similar colloidal properties. This was confirmed by DLS analysis of NP

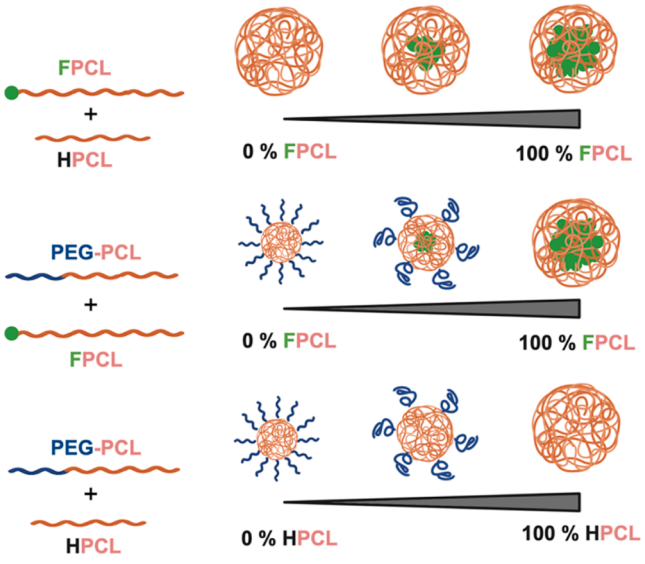

Fig. 2. Schematic representation of the type of NPs obtained depending on the used polymer blend. Depending on the amount of used pegylated polymer, PEG can either assume a brushed (high PEG percentages) or a mushroom (low PEG percentages) like conformation on the NP surface.

dispersions in water at different FPCL percentages showing minor differences both at t0 and over time (1 week aging). Over the analyzed timeframe, all NPs were characterized by a mean hydrodynamic radius (<R_H>) of 80–90 nm with polydispersity indexes (PDI) lower than 0.2 (Fig. 3a). An additional detailed summary of NPs dimensions and PDI is reported in Table S1.

Afterwards, pegylated NPs prepared by mixing PEG-PCL respectively with FPCL and HPCL were systematically investigated to optimize the composition in terms of PEG and fluorination to obtain colloidally stable NPs both in water and in protein containing media. To this aim, two classes of NPs, fluorinated and non-fluorinated, at different percentages of PEG-PCL (0 %, 20 %, 30 %, 50 %, 80 %, 100 %) were prepared and their colloidal properties were characterized in water at t0 and upon aging at 4 °C. NPs showed ZP values ranging from – 40 ± 2 mV to –10 mV ± 6 mV depending on the amount of PEG-PCL in the formulation (from 0 % to 100 %). For highly pegylated NPs colloidal stability comes from steric hindrance and not from electrostatic repulsion. DLS analyses on fresh pegylated dispersions in water showed a consistent R_H reduction at increasing PEG-PCL percentages for both fluorinated and non-fluorinated NPs (Fig. 3b, Table S2). This trend indicates a clear effect of the PEG hydrophilicity on self-assembly, promoting the formation of smaller NPs, in accordance with what reported in the literature [34]. When PEG-PCL is predominant in the formulation, the volume fraction (ϕ) of the hydrophilic block increases with respect to the overall hydrophobic component, thus favoring the formation of micellar-like structures as predicted by the packing parameter [35]. When fully pegylated NPs are prepared (100 % PEG-PCL), micellar like systems are formed (<R_H> of 16 ± 2 nm) (Fig. 3b, Table S2). On the contrary, when either HPCL or FPCL polymers are predominant in the mixture, the contribution of the hydrophilic component (PEG) with respect to the overall hydrophobic component is less significant, thus leading to the formation of NPs with reduced curvature, and increased dimensions (Fig. 3b, Table S2). No consistent differences, in terms of polydispersity, were instead observed. The polydispersity index was lower than 0.2 for all pegylated formulations, indicating good monodispersity of all freshly prepared NPs (Fig. 3b, Table S2).

Regarding the role of fluorine on pegylated NPs, the $(CF_3)_3C$-moiety should not influence the colloidal properties of freshly prepared NPs, in line with the considerations previously made for non-pegylated NPs. DLS analyses of fresh pegylated dispersions in water showed similar R_H distribution and PDI for fluorinated and non-fluorinated NPs at the same percentages of FPCL and HPCL (Fig. 3b, Table S2). However, fluorine could stabilize highly pegylated NPs over time. Considering the intrinsic dynamic nature of PEG-PCL self-assembled micellar-like structures in solution [36], non-covalent *fluorous-fluorous* interactions [37,38] (F···F) should stabilize NPs containing a high percentage of PEG-PCL (contributing more to the hydrophilic ϕ) over time.

In fact, upon a week aging at 4 °C, a consistent increase in the PDI value (0.48) (Fig. 3c, Table S3) and a multimodal R_H distribution – characterized by NPs peak at 16 ± 2 nm and aggregates peaks respectively at 350 ± 35 nm and 2.0 ± 0.2 μm – was observed for 100 % PEG-PCL NPs (Fig. 3d, Table S3). A destabilization of NPs at 80 % of PEG-PCL was also observed, but only for non-fluorinated NPs. 80 % PEG-PCL/HPCL NPs showed a consistent increase in the PDI value (0.33) (Fig. 3c, Table S3) and were characterized by a bimodal R_H distribution with the presence of NPs peak at 36 ± 4 nm and aggregates peak at 400 ± 40 nm (Fig. 3d, Table S3). On the contrary, a lower PDI value (0.17) (Fig. 3c, Table S3) and a monomodal R_H distribution (Fig. 3d, Table S3)

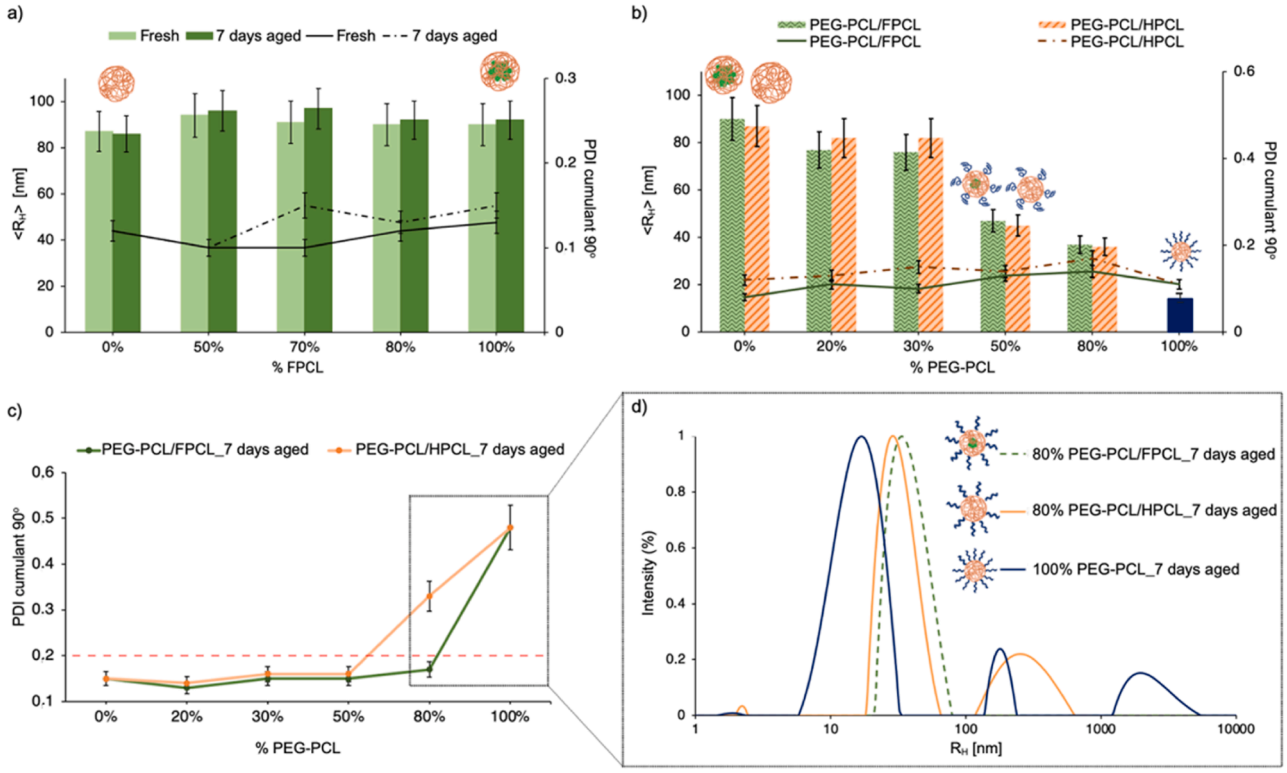

Fig. 3. DLS measurements at θ = 90° of **a**) Non-pegylated NPs at different FPCL/HPCL percentages in water. <R_H> (nm) (histograms), and PDI (lines) of fresh and one-week aged NPs. **b**) Fluorinated and non-fluorinated pegylated NPs at different PEG-PCL percentage. <R_H> (nm) (histograms) and PDI (lines) of fresh samples. **c**) PDI variation of one-week aged samples at 4 °C, showing an increase in polydispersity f°r non-fluorinated NPs containing a percentage of PEG-PCL ≥80 %. **d**) R_H (nm) distribution, respectively, of 80 % PEG-PCL/HPCL, 80 % PEG-PCL/FPCL, and 100 % PEG-PCL NPs upon one week aging at 4 °C. Data showed the presence of a multimodal R_H distribution for both 80 % PEG-PCL/HPCL (orange line) and 100 % PCL-PEG NPs (blue line). 80 % PEG-PCL/FPCL (dotted green line) were instead stable with a monomodal size distribution. All data are obtained as mean (±standard deviation) of three replicates and each replicate is the average of three measurements.

were observed for 80 % PEG-PCL/FPCL NPs. Upon aging, both fluorinated and non-fluorinated NPs at a percentage of PEG-PCL ≤ 50 % were instead stable and monodispersed, as indicated by the maintenance of PDI values lower than 0.2 (Fig. 3c), and no size variation as reported in Table S3.

Fluorination also seemed to stabilize NPs in conditions replicating the cell culture environment. Up to 48 h incubation at 37 °C in DMEM +10 % FBS, 80 % PEG-PCL/FPCL NPs resulted stable and monodispersed as indicated by the presence of a monomodal size distribution both at t0 (<R_H> 36 ± 4 nm) and 48 h incubation (<R_H> 40 ± 4 nm) (Fig. 4a, Table S4) and no variation in PDI values (Fig. 4c, Table S5). On the contrary, 80 % PEG-PCL/HPCL NPs showed a de-stabilization trend with the formation of larger aggregates as indicated by the presence of a bimodal R_H distribution (Fig. 4a, Table S4), and the shift towards higher decay times of the autocorrelation functions (Fig. S1) both at t0 and 48 h incubation. Moreover, a net increase in PDI values after 48 h incubation (Fig. 4b, Table S5) was observed. In accordance with what observed in water, also in protein containing media both fluorinated and non-fluorinated NPs at percentages of PEG ≤ 50 % were stable and monodispersed as indicated by no consistent variation in PDI values up to 48 h incubation in DMEM + 10 % FBS (Fig. 4b,c, Table S5).

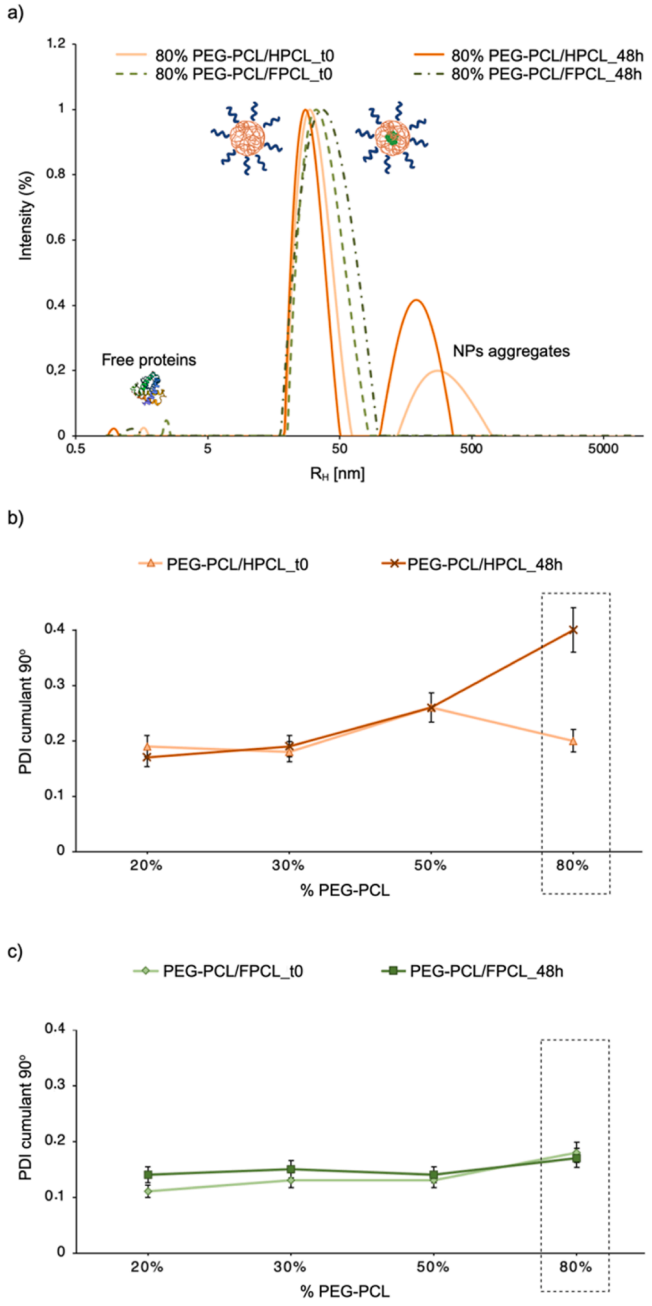

Fig. 4. DLS analysis (θ = 90°) at t0 and after 48 h incubation at 37 °C in DMEM+ 10 % FBS of pegylated NPs. **a**) R_H distribution of 80 % PEG-PCL/HPCL and 80 % PEG-PCL/FPCL NPs. **b**) PDI of non-fluorinated NPs as a function of PEG-PCL percentage. **c**) PDI of fluorinated NPs as a function of PEG-PCL percentage. All data are obtained as mean (± standard deviation) of three replicates and each replicate is the average of three measurements.

The fact that the destabilization of highly pegylated (80 % PEG-PCL) NPs was observed only for non-fluorinated ones confirmed a stabilizing role of non-covalent F···F interactions [37,38]. As previously mentioned, PEG-PCL block copolymers tend to self-assemble into micellar like structures engaging a dynamic equilibrium with the free unimers in aqueous solutions [36]. The thermodynamics and kinetics of this dynamic equilibrium depend on polymer concentration, molecular weight of the copolymer, and molar mass ratio between hydrophilic and hydrophobic segments of PEG-PCL [39,40]. These characteristics make NPs containing a high amount of PEG-PCL (at the fixed molar mass and PEG/PCL ratio selected for this study) likely to be prone to destabilization over time and when in contact with environments potentially influencing colloidal stability (e.g., proteins and salt containing media). This destabilization seems to be compensated for FPCL NPs. In fact, when in the formulation mixture a low amount of FPCL (20 %) instead of HPCL is present together with PEG-PCL, F···F interactions are likely to promote the formation of NPs with a more packed hydrophobic core. Therefore, the dynamicity and reversibility of the self-assembly is reduced, resulting in an improved stability of NPs.

NPs stability over time and in physiological conditions is essential for biological application. At the same time, to prepare NPs that can be used as drug delivery systems potentially detectable by ^{19}F NMR, a suitable amount of fluorine atoms is mandatory for addressing the detection threshold. Additionally, for in vivo application stealth properties are usually required to avoid NPs fast clearance. For these reasons, we decided to focus only on the formulations balancing a high amount of fluorinated and pegylated polymers. Specifically, only 20 % and 50 % PEG-PCL/FPCL NPs were selected for further studies.

3.2.1. *Protein corona and cytotoxicity studies*

PC characterization was aimed at optimizing the composition in terms of PEG-PCL for obtaining stealth NPs for potential further in vivo application (Fig. 5a). Reducing the interaction between NP and proteins is considered a key point for the development of effective drug delivery systems. Non-fluorinated 20 % and 50 % PEG-PCL/HPCL NPs were analyzed as control to confirm the hypothesis that for our systems fluorine would not have any influence on PC formation due to its localization in NPs inner core. DLS analysis confirmed the stability of the isolated PC-NP complexes as indicated by the maintenance of a monomodal size distribution and no increase in PDI values (Table S6). The lack of changes in the autocorrelation functions of the isolated PC-NPs complexes compared to NPs in water (Fig. S2) supports the complete stability of the isolated complexes and the effectiveness of the used isolation protocol.

SDS-PAGE showed no differences in PC composition between fluorinated and non-fluorinated NPs (Fig. 5b), confirming that NPs self-assemble shielding fluorine in their inner core. Moreover, NPs with only 20 % PEG-PCL showed a tendency to form a consistent PC, as indicated by the presence of different protein bands in the gel (Fig. 5b) and increased R_H (Table S6). This suggests that stealth conditions require a higher PEG density for these NPs (Fig. 5a,b). On the contrary, NPs with 50 % PEG-PCL showed a net reduction of PC, as indicated by the presence of a single protein band in the gel in correspondence of 75 kDa (probably related to albumin or fibrinogen) (Fig. 5b), and no significative variation in the hydrodynamic size distribution (Table S6). This suggests that 50 % PEG-PCL can be considered a good compromise

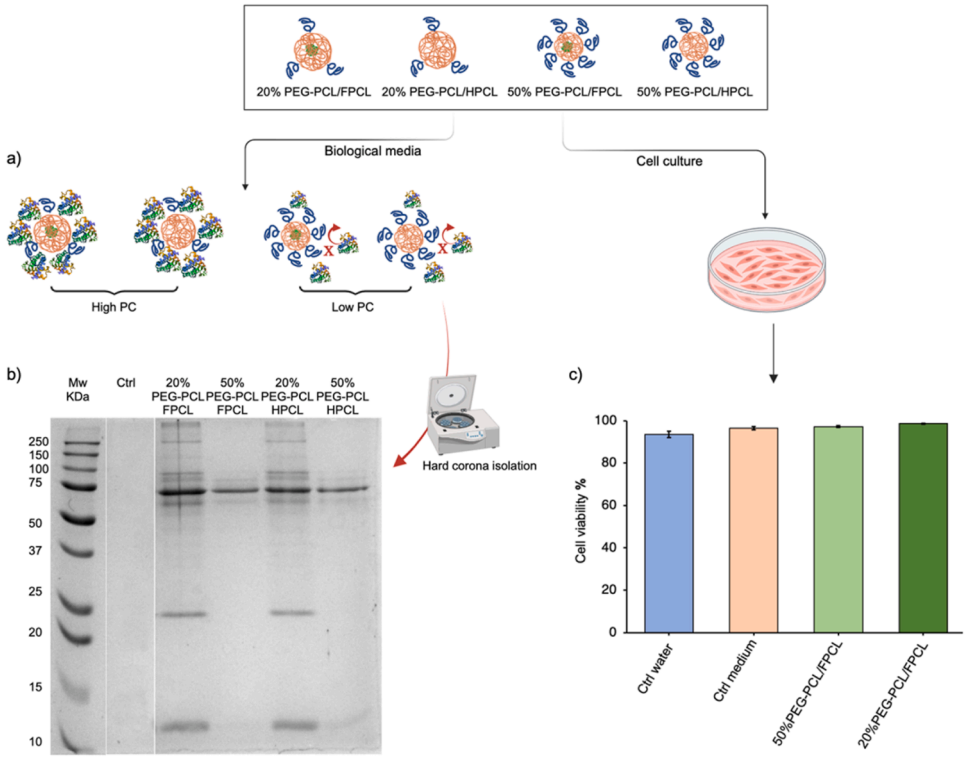

Fig. 5. **a**) Schematic representation of the mechanism of PC formation on NPs containing different percentages of PEG-PCL, **b**) SDS-PAGE of NP-PC complexes isolated upon 1 h incubation at 37 °C of fluorinated and non-fluorinated pegylated NPs in DMEM + 10 % FBS. **c**) Cell viability evaluated by flow cytometry upon 24 h cell incubation with 50 % and 20 % PEG-PCL/FPCL NPs. Standard deviations refer to a single batch of NPs for which each measurement was repeated three times.

to confer NPs with improved stealth properties.

NPs cytotoxicity was evaluated upon 24 h cell incubation. Both 20 % PEG-PCL/FPCL and 50 % PEG-PCL/FPCL NPs showed to be highly biocompatible, with levels of cell viability higher than 90 % and comparable to those of non-treated controls in water and culture medium (Fig. 5c). Considering the acknowledged importance of NPs stealth properties for in vivo drug delivery, 50 % PEG-PCL/FPCL NPs were selected as the most promising ones and their efficacy as drug carriers was subsequently proven by testing their ability to encapsulate the hydrophobic drug dexamethasone (DEX).

3.3. Drug loaded NPs formulation and characterization

Drug-loaded 50 % PEG-PCL/FPCL (DEX@PEG-PCL/FPCL) NPs were formulated using the same nanoprecipitation method used for drug-free NPs, adding DEX to the organic solution. Non-fluorinated drug-loaded 50 % PEG-PCL/HPCL NPs (DEX@PEG-PCL/HPCL) were used as control to investigate if the presence of fluorine could improve drug loading efficacy. First, NPs colloidal properties were characterized by DLS. The former analysis did not show significant changes in size and PDI between the two prepared formulations as well as with respect to unloaded NPs (Table 2). Obtained size distributions were characterized by $<R_H>$ of 42 ± 4 nm for DEX@PEG-PCL/FPCL and 46 ± 5 nm for DEX@PEG-PCL/HPCL (Table 2, Figs. S3a,b). Moreover, in accordance with what observed for empty NPs, DEX loaded NPs are stable in culture medium with the presence of proteins up to 48 h incubation, as indicated by no variation in autocorrelation functions (Figs. S3c,d). TEM analysis on DEX@PEG-PCL/FPCL in water (Fig. S4) confirmed the spherical shape of developed NPs and the resulting size distribution is in accordance with DLS data.

DEX loading (encapsulation efficacy, EE% and drug loading capacity, DL%) was quantitatively evaluated by HPLC analysis, showing effective results with no significant differences between fluorinated and non-fluorinated NPs (Table 2). The obtained values of EE% and DL% are comparable with what reported in the literature for similar systems [13, 41].

Finally, to evaluate the potential efficiency of DEX@PEG-PCL/FPCL NPs as detectable drug delivery systems, a quantitative ^{19}F NMR spectrum was acquired and longitudinal (T_1) and transverse (T_2) relaxation times were evaluated. Drug-free NPs were analyzed as control. Quantitative ^{19}F NMR spectra showed the presence of a characteristic sharp, intense, and single peak at - 66.7 ppm for both DEX-loaded and drug-

Table 2
DLS analysis of 50 % PEG-PCL/FPCL, 50 % PEG-PCL/HPCL, DEX@PEG-PCL/FPCL and DEX@PEG-PCL/HPCL NPs. DL% and EE% of DEX@PEG-PCL/FPCL and DEX@PEG-PCL/HPCL NPs are reported.

	50% PEG-PCL/FPCL	50% PEG-PCL/HPCL	DEX@PEG-PCL/FPCL	DEX@PEG-PCL/HPCL
$< R_H >$[nm][1*]	45 ± 4	43 ± 4	42 ± 4	46 ± 5
PDI[2*]	0.13 ± 0.01	0.14 ± 0.01	0.10 ± 0.01	0.12 ± 0.01
DL%[3*]	/	/	3.0 ± 0.1	3.0 ± 0.2
EE%[4*]	/	/	98 ± 1	99 ± 2

[1]The $< R_H >$ is referred to the intensity weighted size distribution deriving from CONTIN analysis of DLS measurements at θ = 90°.
[2]The polydispersity index was obtained by cumulant fitting of DLS measurements at θ = 90°.
[3,4]Drug loading (DL%) and encapsulation efficiency (EE%) deriving from HPLC quantification.
*All data are obtained as mean (±standard deviation) of three replicates and each replicate is the average of three measurements.

free NPs (Fig. S5). Drug-loaded and drug-free NPs showed T_1 values, respectively, of 512 *ms* and 517 *ms* and T_2 values respectively of 100 *ms* and 93 *ms*, suggesting that self-assembly and drug loading processes did not impair the mobility of the fluorinated chains, thus not affecting ^{19}F NMR activity. These results are promising also considering that in the literature, for similar systems containing a comparable amount of encapsulated drug, a consistent reduction of T_2 upon drug loading was instead reported [13]. For this reason, drug-loaded NPs prepared by mixing 50 % PEG-PCL and 50 % FPCL can be considered a new class of drug delivery vectors potentially detectable by ^{19}F NMR.

4. Conclusions

In summary, a comprehensive study on self-assembly properties and PC formation of HPCL, FPCL and PCL-PEG based NPs as a function of fluorination and pegylation has been reported. This allowed to define NPs based on 50 % PEG-PCL/FPCL as a new class of promising stealth and ^{19}F NMR sensitive drug delivery vectors. NP ability to work as drug carriers was proven by testing their ability to encapsulate the hydrophobic drug dexamethasone (DEX). NPs showed to be colloidally stable in physiological conditions and in culture medium, to form a reduced protein corona, and to encapsulate drug payloads in line with what reported in the literature. Moreover, NPs ^{19}F NMR properties are not impaired by the drug loading process. Taking into account these preliminary results, we believe that 50 % PEG-PCL/FPCL NPs could be potential candidates as multifunctional drug delivery vehicles.

CRediT authorship contribution statement

Baldelli Bombelli Francesca: Writing – review & editing, Writing – original draft, Supervision, Investigation, Funding acquisition, Data curation, Conceptualization. **Cellesi Francesco:** Writing – review & editing, Writing – original draft, Supervision, Methodology, Investigation, Funding acquisition, Data curation, Conceptualization. **Pipino Christian:** Methodology, Data curation. **Chirizzi Cristina:** Writing – review & editing, Methodology, Investigation, Data curation. **Lagarrigue Prescillia:** Writing – review & editing, Methodology, Investigation, Data curation. **Metrangolo Pierangelo:** Writing – review & editing, Supervision, Funding acquisition, Data curation. **Bona Beatrice Lucia:** Writing – review & editing, Writing – original draft, Methodology, Investigation, Conceptualization. **Martinez Espinoza Maria Isabel:** Methodology, Data curation.

Declaration of Competing Interest

The authors declare that they have no known competing financial interests or personal relationships that could have appeared to influence the work reported in this paper.

Data Availability

Data will be made available on request.

Acknowledgements

The authors are thankful to the NEWMED project, ID: 1175999 (funded by Regione Lombardia, POR FESR 2014 2020) and to the INNOVA project (funded by Ministero della Salute, PNC-E3-2022-23683266). The authors are grateful to colleagues for their technical support, particularly Serena Pellegatta PhD, for providing access to the biology laboratory of the Molecular Neuro-Oncology Unit at Fondazione IRCCS Istituto Neurologico Carlo Besta, Milan, Italy, and Dr. Daniela Lisini from the same Institute for generously providing mesenchymal stem cells for in vitro experiments. The figures were made using BioRender.com.

Appendix A. Supporting information

Supplementary data associated with this article can be found in the online version at doi:10.1016/j.colsurfb.2023.113730.

References

[1] M.J. Mitchell, M.M. Billingsley, R.M. Haley, M.E. Wechsler, N.A. Peppas, R. Langer, Engineering precision nanoparticles for drug delivery, Nat. Rev. Drug Discov. 20 (2021) 101–124.
[2] S. Đorđević, M.M. Gonzalez, I. Conejos-Sánchez, B. Carreira, S. Pozzi, R.C. Acúrcio, R. Satchi-Fainaro, H.F. Florindo, M.J. Vicent, Current hurdles to the translation of nanomedicines from bench to the clinic, Durg Deliv. Transl. Res. 12 (2022) 500–525.
[3] S.-J. Lee, H.-J. Kim, Y.-M. Huh, I.W. Kim, J.H. Jeong, J.-C. Kim, J.-D. Kim, Functionalized magnetic PLGA nanospheres for targeting and bioimaging of breast cancer, J. Nanosci. Nanotechnol. 18 (2018) 1542.
[4] Y. Li, M. Wu, N. Zhang, C. Tang, P. Jiang, X. Liu, F. Yan, H. Zheng, Mechanisms of enhanced antiglioma efficacy of polysorbate 80-modified paclitaxel-loaded PLGA nanoparticles by focused ultrasound, J. Cell. Mol. Med. 22 (2018) 4171–4182.
[5] E.R. Swy, A.S. Schwartz-Duval, D.D. Shuboni, M.T. Latourette, C.L. Mallet, M. Parys, D.P. Cormode, E.M. Shapiro, Dual-modality, fluorescent, PLGA encapsulated bismuth nanoparticles for molecular and cellular fluorescence imaging and computed tomography, Nanoscale 6 (2014) 13104–13112.
[6] J.M. Arango, D. Padro, J. Blanco, S. Lopez-Fernandez, P. Castellnou, P. Villa-Valverde, J. Ruiz-Cabello, A. Martin, M. Carril, Fluorine labeling of nanoparticles and in vivo 19F magnetic resonance imaging, ACS Appl. Mater. Interfaces 13 (2021) 12941–12949.
[7] C. Zhang, S.S. Moonshi, W. Wang, H.T. Ta, Y. Han, F.Y. Han, H. Peng, P. Král, B. E. Rolfe, J.J. Gooding, K. Gaus, A.K. Whittaker, High F-content perfluoropolyether-based nanoparticles for targeted detection of breast cancer by ^{19}F magnetic resonance and optical imaging, ACS Nano 12 (2018) 9162–9176.
[8] I. Tirotta, V. Dichiarante, C. Pigliacelli, G. Cavallo, G. Terraneo, F. Baldelli Bombelli, P. Metrangolo, G. Resnati, 19)F magnetic resonance imaging (MRI): from design of materials to clinical applications, Chem. Rev. 115 (2015) 1106–1129.
[9] T. Wu, A. Li, K. Chen, X. Peng, J. Zhang, M. Jiang, S. Chen, X. Zheng, X. Zhou, Z.-X. Jiang, Perfluoro-*tert*-butanol: a cornerstone for high performance fluorine-19 magnetic resonance imaging, Chem. Commun. 57 (2021) 7743–7757.
[10] M.S. Fox, J.M. Gaudet, P.J. Foster, Fluorine-19 MRI contrast agents for cell tracking and lung imaging, Magn. Reson. Insight 8 (2015) 53–67.
[11] O. Koshkina, P.B. White, A.H.J. Staal, R. Schweins, E. Swider, I. Tirotta, P. Tinnemans, R. Fokkink, A. Veltien, N.K. van Riessen, E.R.H. van Eck, A. Heerschap, P. Metrangolo, F. Baldelli Bombelli, Nanoparticles for "two color" ^{19}F magnetic resonance imaging: towards combined imaging of biodistribution and degradation, J. Colloid Interface Sci. 565 (2020) 278–287.
[12] J. Ruiz-Cabello, B.P. Barnett, P.A. Bottomley, J.W.M. Bulte, Fluorine (19F) MRS and MRI in biomedicine, NMR Biomed. 24 (2011) 114–129.
[13] G. Neri, G. Mion, A. Pizzi, W. Celentano, L. Chaabane, M.R. Chierotti, R. Gobetto, M. Li, P. Messa, F. De Campo, F. Cellesi, P. Metrangolo, F. Baldelli, Bombelli, fluorinated PLGA nanoparticles for enhanced drug encapsulation and ^{19}F NMR detection, Chem. – Eur. J. 26 (2020) 10057–10063.
[14] W. Celentano, G. Neri, F. Distante, M. Li, P. Messa, C. Chirizzi, L. Chaabane, F. De Campo, P. Metrangolo, F. Baldelli Bombelli, F. Cellesi, Design of fluorinated hyperbranched polyether copolymers for 19F MRI nanotheranostics, Polym. Chem. 11 (2020) 3951.
[15] L. Zerillo, K.B.S.S. Gupta, F.A.W.M. Lefeber, C.G. Da Silva, F. Galli, A. Chan, A. Veltien, W. Dou, R. Censi, P. Di Martino, M. Srinivas, L. Cruz, Novel fluorinated poly (lactic-co-glycolic acid) (PLGA) and polyethylene glycol (PEG) nanoparticles for monitoring and imaging in osteoarthritis, Pharmaceutics 13 (2021) 235.
[16] B.L. Bona, O. Koshkina, C. Chirizzi, V. Dichiarante, P. Metrangolo, F. Baldelli Bombelli, Multibranched-based fluorinated materials: tailor-made design of ^{19}F-MRI probes, Acc. Mater.. Res. 4 (2023) 71–85.
[17] T. Song, Y. Gao, M. Song, J. Qian, H. Zhang, J. Zhou, Y. Ding, Fluoropolymers-mediated efficient biomacromolecule drug delivery, Med. Drug Discov. 14 (2022) 100123.
[18] J. Lv, B. He, J. Yu, Y. Wang, C. Wang, S. Zhang, H. Wang, J. Hu, Q. Zhang, Y. Cheng, Fluoropolymers for intracellular and in vivo protein delivery, Biomaterials 182 (2018) 167–175.
[19] G. Rong, C. Wang, L. Chen, Y. Yan, Y. Cheng, Fluoroalkylation promotes cytosolic peptide delivery, Sci. Adv. 6 (2020) 1774.
[20] Z. Zhang, W. Shen, J. Ling, Y. Yan, J. Hu, Y. Cheng, The fluorination effect of fluoroamphiphiles in cytosolic protein delivery, Nat. Commun. 9 (2018) 1377.
[21] J. Lv, Y. Cheng, Fluoropolymers in biomedical applications: state-of-the-art and future perspectives, Chem. Soc. Rev. 50 (2021) 5435–5467.
[22] A. Behl, V.S. Parmar, S. Malhotra, A.K. Chhillar, Biodegradable diblock copolymeric PEG-PCL nanoparticles: synthesis, characterization and applications as anticancer drug delivery agents, Polymer 207 (2020) 122901.
[23] W. Celentano, M. Pizzocri, F. Moncalvo, F. Pessina, M. Matteoli, F. Cellesi, L. Passoni, Functional poly(ε-caprolactone)/poly(ethylene glycol) copolymers with complex topologies for doxorubicin delivery to a proteinase-rich tumor environment, ACS Appl. Polym. Mater. 4 (2022) 8043–8056.
[24] W. Celentano, S. Ordanini, R. Bruni, L. Marocco, P. Medaglia, A. Rossi, S. Buzzaccaro, F. Cellesi, Complex poly(ε-caprolactone)/poly(ethylene glycol)

copolymer architectures and their effects on nanoparticle self-assembly and drug nanoencapsulation, Eur. Polym. J. 144 (2021) 110226.
[25] M.N. Vu, H.G. Kelly, A.K. Wheatley, S. Peng, E.H. Pilkington, N.A. Veldhuis, T. P. Davis, S.J. Kent, N.P. Truong, Cellular interactions of liposomes and PISA nanoparticles during human blood flow in a microvascular network, Small 16 (2020) 2002861.
[26] D. Di Silvio, N. Rigby, B. Bajka, A. Mayes, A. Mackie, F. Baldelli Bombelli, Technical tip: high-resolution isolation of nanoparticle–protein corona complexes from physiological fluids, Nanoscale 7 (2015) 11980–11990.
[27] S. Palchetti, V. Colapicchioni, L. Digiacomo, G. Caracciolo, D. Pozzi, A.L. Capriotti, G. La Barbera, A. Laganà, The protein corona of circulating PEGylated liposomes, Biochim. Et. Biophys. Acta (BBA)-Biomembr. 1858 (2016) 189–196.
[28] D. Docter, U. Distler, W. Storck, J. Kuharev, D. Wünsch, A. Hahlbrock, S.K. Knauer, S. Tenzer, R.H. Stauber, Quantitative profiling of the protein coronas that form around nanoparticles, Nat. Protoc. 9 (2014) 2030–2044.
[29] D. Lisini, S. Nava, S. Frigerio, S. Pogliani, G. Maronati, A. Marcianti, V. Coccè, G. Bondiolotti, L. Cavicchini, F. Paino, F. Petrella, G. Alessandri, E.A. Parati, A. Pessina, Automated large-scale production of paclitaxel loaded mesenchymal stromal cells for cell therapy applications, Pharmaceutics 12 (2020) 411–426.
[30] S. Ordanini, W. Celentano, A. Bernardi, F. Cellesi, Mannosylated brush copolymers based on poly(ethylene glycol) and poly(ε-caprolactone) as multivalent lectin-binding nanomaterials, Beilstein J. Nanotechnol. 10 (2019) 2192–2206.
[31] S. Witt, T. Scheper, J.-G. Walter, Production of polycaprolactone nanoparticles with hydrodynamic diameters below 100 nm, Eng. Life Sci. 19 (2019) 658–665.
[32] K.S. Shalaby, M.E. Soliman, G. Bonacucina, M. Cespi, G.F. Palmieri, O.A. Sammour, A.A. El Shamy, L. Illum, L. Casettari, Nanoparticles based on linear and star-shaped poly(ethylene glycol)-poly(ε-caprolactone) copolymers for the delivery of antitubulin drug, Pharm. Res. 33 (2016) 2010–2024.
[33] R. Gref, M. Lück, P. Quellec, M. Marchand, E. Dellacherie, S. Harnisch, T. Blunk, R. H. Müller, Stealth' corona-core nanoparticles surface modified by polyethylene glycol (PEG): influences of the corona (PEG chain length and surface density) and of the core composition on phagocytic uptake and plasma protein adsorption, Colloids Surf. B: Biointerfaces 18 (2000) 301–313.
[34] Y. Hu, J. Xie, Y.W. Tong, C.-H. Wang, Effect of PEG conformation and particle size on the cellular uptake efficiency of nanoparticles with the HepG2 cells, J. Control. Release 118 (2007) 7–17.
[35] P. Grossen, D. Witzigmann, S. Sieber, J. Huwyler, PEG-PCL-based nanomedicines: a biodegradable drug delivery system and its application, J. Control. Release 260 (2017) 46–60.
[36] M.S. Sadeghi, M.R. Moghbeli, W.A. Goddard III, Self-assembly mechanism of PEG-b-PCL and PEG-b-PBO-b-PCL amphiphilic copolymer micelles in aqueous solution from coarse grain modeling, J. Polym. Sci. 59 (2021) 614–626.
[37] M. Cametti, B. Crousse, P. Metrangolo, R. Milani, G. Resnati, The fluorous effect in biomolecular applications, Chem. Soc. Rev. 41 (2012) 31–42.
[38] C. Pigliacelli, A. Acocella, I. Díez, L. Moretti, V. Dichiarante, N. Demitri, H. Jiang, M. Maiuri, R.H.A. Ras, F. Baldelli Bombelli, G. Cerullo, F. Zerbetto, P. Metrangolo, G. Terraneo, High-resolution crystal structure of a 20 kDa superfluorinated gold nanocluster, Nat. Commun. 13 (2022) 2607.
[39] M. Ghezzi, S. Pescina, C. Padula, P. Santi, E. Del Favero, L. Cantù, S. Nicoli, Polymeric micelles in drug delivery: an insight of the techniques for their characterization and assessment in biorelevant conditions, J. Control. Release 332 (2021) 312–336.
[40] S.C. Owen, D.P.Y. Chan, M.S. Shoichet, Polymeric micelle stability, Nano Today 7 (2012) 53–65.
[41] C. Gómez-Gaete, E. Fattal, L. Silva, M. Besnard, N. Tsapis, Dexamethasone acetate encapsulation into Trojan particles, J. Control. Release 128 (2008) 41–49.